5
Signal Conditioning and Preprocessing

R. Gutierrez-Osuna, H. Troy Nagle, B. Kermani, Susan S. Schiffman

5.1
Introduction

The topics covered in this chapter establish the connection between gas sensors and pattern recognition, the two fundamental modules of an odor-sensing instrument that are covered in Chapters 4 and 6, respectively. A number of electronic circuits are involved in integrating pattern analysis algorithms with the underlying chemical transduction mechanisms, as shown in Fig. 5.1. First, the response of the odor sensors (e.g., a resistance change) needs to be measured and converted into an electrical signal (e.g., a voltage). This operation is performed by means of interface circuits. Second, the electrical signal undergoes analog conditioning (e.g., filtering) to enhance its information content. Third, the analog signal is sampled, digitized and stored in computer memory (not covered in this chapter due to space constraints). Finally, the sampled signal is digitally preprocessed (e.g., autoscaling) in order to make it suitable for pattern analysis.

This chapter is organized in three basic parts: interface circuits, signal conditioning, and preprocessing. Section 5.2 presents the fundamental interface circuits for the three primary odor sensor types: resistive, piezoelectric, and field-effect. Section 5.3 reviews the primary functions performed by analog signal conditioning circuits. Section 5.4 covers data preprocessing – the first stage of digital signal processing. The issue of sensor and instrumentation noise, one of the most important factors determining electronic-nose performance, is also reviewed in Section 5.5. The chapter con-

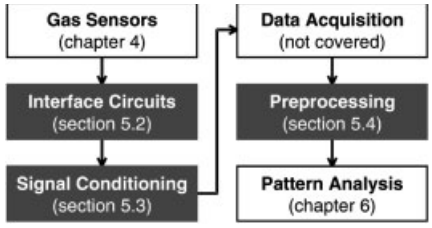

Fig. 5.1 Organization of this chapter

Handbook of Machine Olfaction: Electronic Nose Technology.
Edited by T.C. Pearce, S.S. Schiffman, H.T. Nagle, J.W. Gardner

ISBN: 3-527-30358-8

cludes with a review of current instrumentation trends aimed at increasing the selectivity of odor sensor systems.

5.2 Interface Circuits

Sensor interface circuits constitute the first stage of electronic instrumentation. The purpose of these circuits is to generate an electrical signal that reflects changes in the sensors. Since interface circuits are tightly coupled to the underlying sensing technology, we will focus our presentation on three widely used odor sensors: conductivity (metal-oxide and conductive-polymer chemoresistors), piezo-electric (surface acoustic wave and quartz crystal microbalance), and field effects (metal-oxide field-effect transistors). In addition, this section reviews the issue of operating temperature control, essential for the operation of metal-oxide transducers.

5.2.1 Chemoresistors

In chemoresistive sensors the presence of volatile compounds changes the conductance (or resistance) of the sensing membrane. Interface circuits for these sensors are, therefore, relatively simple since they only involve measuring resistance changes. Two types of resistance measurement circuits are commonly used: voltage dividers and Wheatstone bridges. These circuits are presented and analyzed in the following subsections. Linear versions of these circuits that involve operational amplifiers are presented in section 5.3.5 as a special type of analog signal conditioning. Finally, AC impedance measurement techniques for chemoresistors are briefly reviewed at the end of this section.

5.2.1.1 Voltage Dividers

The standard method for measuring large resistance changes is a voltage divider, as shown in Fig. 5.2a. This instrumentation circuit is very popular due to its simplicity. The resistive sensor is placed in series with a load resistor R_L and connected to a voltage reference V_{CC}. The current through the sensitive element and load resistance becomes:

$$I_S = \frac{V_{CC}}{R_S + R_L} \tag{1}$$

Changes in sensor resistance are then measured as voltage changes across the sensor (V_S) or the load resistor (V_L). For convenience, we will use the voltage across the load resistor since it is a single-ended measurement and the subsequent derivation becomes simpler. Using Ohm's Law ($V = IR$), the resulting output voltage becomes:

$$V_L = I_S R_L = \frac{V_{CC}}{R_S + R_L} R_L \tag{2}$$

The value of the load resistor should be selected to maximize the sensitivity of the circuit, that is, the slope of the $V_L - R_S$ curve, which can be calculated as:

$$S = \frac{\partial V_L}{\partial R_S} = \frac{\partial}{\partial R_S}\left(\frac{R_L}{R_S + R_L} V_{CC}\right) = V_{CC} \frac{-R_L}{(R_S + R_L)^2} \tag{3}$$

The maximum of the selectivity is finally determined by finding the zeros of its partial derivative with respect to R_L:

$$\frac{dS}{dR_L} = \frac{\partial}{\partial R_L}\left(\frac{-R_L}{(R_S + R_L)^2} V_{CC}\right) = 0 \tag{4}$$

It can be shown that the optimal load resistor is $R_L = R_S$, this is the sensor resistance at the operating point, typically defined by a reference gas (e.g., clean air). The voltage divider is the circuit recommended by several metal-oxide sensor manufacturers [1, 2] but it has several shortcomings. First, the relationship between the sensor resistance R_S and the output voltage V_L is nonlinear since the current I_S through the sensor depends not only on the load resistor but also on the sensor resistance (refer to section 5.3.5.1 for linearization circuits). Second, and more importantly, the circuit is only appropriate for measuring large resistance changes, such as those typical of metal-oxide sensors. Conducting polymer chemoresistors have sensitivities one order of magnitude lower [3] and require the use of Wheatstone bridges.

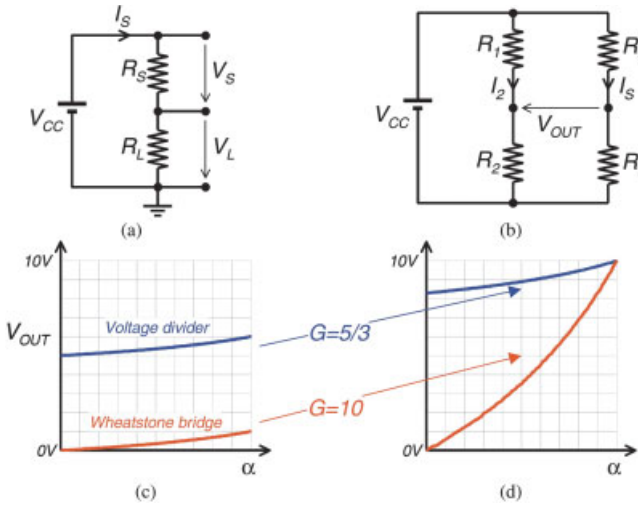

Fig. 5.2 (*a*) Voltage divider and (*b*) Wheatstone bridge for resistive sensors. (*c*–*d*) Sensitivity improvements with a gain stage

5.2.1.2 The Wheatstone Bridge

When the resistance changes to be measured are small relative to the baseline resistance of the sensor, the information in the output voltage will consist of small fluctuations superimposed on a large offset voltage. Although the sensitivity can be boosted with a gain stage, the problem remains since a large portion of the dynamic range of the ADC will be 'wasted' in measuring the offset voltage. One solution for measuring small resistance changes is to subtract the offset voltage with a second voltage divider, as shown in Fig. 5.2b. The differential voltage in the bridge is:

$$V_{Out} = R_L I_S - R_2 I_2 = R_L \frac{V_{CC}}{R_S + R_L} - R_2 \frac{V_{CC}}{R_1 + R_2} = V_{CC}\left(\frac{R_L}{R_S + R_L} - \frac{R_2}{R_1 + R_2}\right) \quad (5)$$

As in the voltage divider of Fig. 5.2a, sometimes called a half-bridge circuit, the maximum sensitivity for the Wheatstone bridge is obtained by choosing resistors R_1, $R_2$and R_L equal to the sensor baseline resistance. This measurement approach is known as a deflection method, because the sensor response is measured as a differential voltage when the bridge becomes unbalanced. An alternative approach, known as the null method, consists of adjusting the resistors R_1, and R_2 to cancel the differential voltage V_{OUT}. The sensor resistance is then obtained from the balance condition:

$$V_{OUT} = 0 \leftrightarrow \frac{R_1}{R_2} = \frac{R_S}{R_L} \rightarrow R_S = R_L \frac{R_1}{R_2} \quad (6)$$

By comparing Eqs. (5) and (6) it can be inferred that, unlike deflection measurements, the null method is insensitive to fluctuations in the supply voltage. The deflection method, on the other hand, is easier to implement and yields faster responses, making it more appealing for dynamic measurements.

It must be noted that the Wheatstone bridge (deflection-method) has the same sensitivity as a voltage divider. Notice that the only difference between Eqs. (2) and (5) is the offset voltage provided by the $R_1 - R_2$ arm, which does not depend on the sensor resistance. The main advantage of the Wheatstone bridge is that it affords higher amplification gains since the offset voltage has already been removed. To illustrate this point, assume a gas sensor that has a resistance that decreases in the presence of an odor, $R_S = R_0(1 - \alpha)$. Figure 5.2c shows the response of both circuits for $Ø = \leq \alpha \leq 1/3$, $R_1 = R_2 = R_L = R_0$, and $V_{CC} = 10$V. If this signal is to be captured with a data acquisition system that has a dynamic range of 0 V to 10 V, the maximum gain that can be applied to the voltage divider is only 5/3. Although the Wheatstone bridge has the same initial sensitivity (slope), removal of the baseline offset allows a maximum gain of 10, as shown in Fig. 5.2d. The figure also illustrates the nonlinearity introduced by the deflection measurements.

It is important to mention that voltage dividers and Wheatstone bridges can be used to remove common-mode effects by replacing the load resistor R_L with a reference sensor that is shielded from the variable being sensed by the primary sensor but unshielded from environmental conditions. This approach is widely employed in strain gages to compensate for temperature interference, and in pellistors for both tempera-

ture and humidity compensation [4]. The linearized voltage dividers covered in section 5.3.5.1 are also commonly used for compensation purposes. These types of measurements, based on the ratio between a primary sensor and a reference sensor, are known as ratiometric techniques [5].

5.2.1.3 AC Impedance Spectroscopy

Impedance spectroscopic techniques are commonly used to determine the contribution of the different structures in a device (e.g., surface, bulk, grain, and contacts). Impedance spectroscopy is performed by applying a small-amplitude AC voltage to the sensor and measuring the resulting current. By sweeping the frequency of the AC signal and measuring the impedance at multiple frequencies, an equivalent electrical model can be derived that reveals the contributions of each structure for different gases [6, 7]. Impedance spectroscopy requires specialized (and expensive) test and measurement equipment such as impedance analyzers or frequency response analyzers.

Several studies have proposed the use of impedance spectroscopy to improve the selectivity of chemoresistors. Weimar and Göpel [8] have employed two-point measurements at frequencies between 1 Hz and 1 MHz to extract the complex impedance of a custom tin-oxide sensor with interdigitated electrodes. Figure 5.3a shows the Cole-

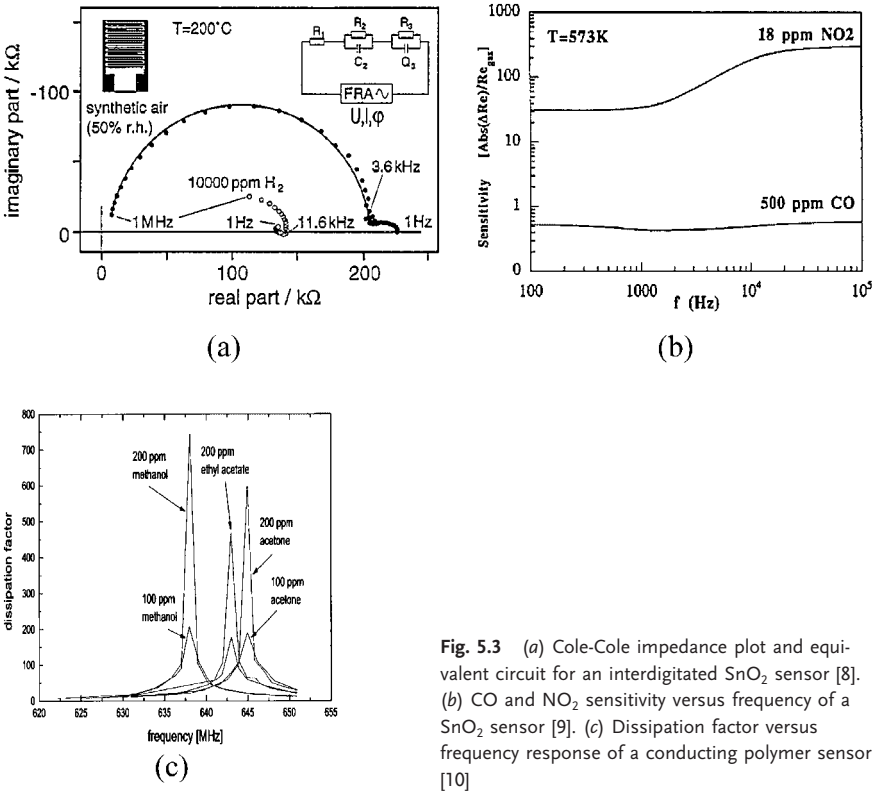

Fig. 5.3 (*a*) Cole-Cole impedance plot and equivalent circuit for an interdigitated SnO_2 sensor [8]. (*b*) CO and NO_2 sensitivity versus frequency of a SnO_2 sensor [9]. (*c*) Dissipation factor versus frequency response of a conducting polymer sensor [10]

Cole impedance plot of a sensor exposed to pure carrier gas, before and after the addition of 10 000 ppm H_2. The parameters of the equivalent electrical circuit shown in the upper right corner of the figure were obtained by fitting the impedance model $R_1 + R_2 \| C_2 + R_3 \| Q_3$ (solid line) to the experimental data (dotted). The resistance R_1 models contributions from the bulk and the surface of the tin oxide. Contribution from the SnO_2/Pt contacts are modeled by only one parallel component (R_2, C_2) since the two-point setup cannot separate the impedance of the two electrodes. These contact contributions are responsible for the large semicircle in the figure. The third contribution (R_3, Q_3), caused by migration of surface species along the grain boundaries at low frequencies, is responsible for the small semicircle in the impedance plot. This contribution becomes inductive in the presence of H_2 (notice that the small semicircle is mirrored with respect to the one for synthetic air). This study indicates that sensitivity to CO, NO_2, and H_2 can be improved by measuring the AC impedance of the sensor at DC, 3 kHz, and 20 kHz, respectively. Qualitatively similar conclusions, shown in Fig. 5.3b have been reported [9]. Amrani et al. [10] have performed impedance spectroscopy at higher frequencies (100–1000 MHz) to characterize conducting polymer sensors. Their results, summarized in Fig. 5.3c, indicate that methanol, ethyl acetate, and acetone (with dipole moments of 1.69 μD, 1.78 μD and 2.88 μD, respectively) induce peaks in the dissipation factor (the ratio of resistance to reactance, R/X_C) at different frequencies, with the peak amplitude being a monotonically increasing function of the vapor concentration.

5.2.2 Acoustic Wave Sensors

Instrumentation electronics for acoustic wave gas sensors are more complex than those employed for chemoresistors, as they involve AC signals of high frequency (e.g., MHz range). According to the number of piezo-electric transducers used in the device, acoustic wave sensors can be classified into one-port and two-port devices:

- One-port devices consist of a single transducer that is used both as an input and as an output. The port is used to generate an acoustic signal, which is combined with the charges induced in the device to produce a measurable impedance change, or a shift in resonance frequency if using an oscillator circuit. A representative sensor for this type of device is the QMB, also known as a thickness-shear mode sensor.
- Two-port devices, as the name indicates, have separate inputs and outputs. An input interdigitated transducer (IDT) is used to induce an acoustic signal, which propagates across the surface of the device. When the acoustic wave reaches the output transducer, an electrical signal is regenerated, and its phase and/or amplitude changes with respect to the input signal are used as measurement variables. A representative two-port device is the SAW delay line sensor[a].

a) One-port or resonant SAW sensor configurations are also employed. A single IDT is placed in the center of the device and mechanical 'grooves' are micro-fabricated on the edges of the substrate to reflect the acoustic waves back to the IDT, creating a 'resonant cavity' in the center of the device [12].

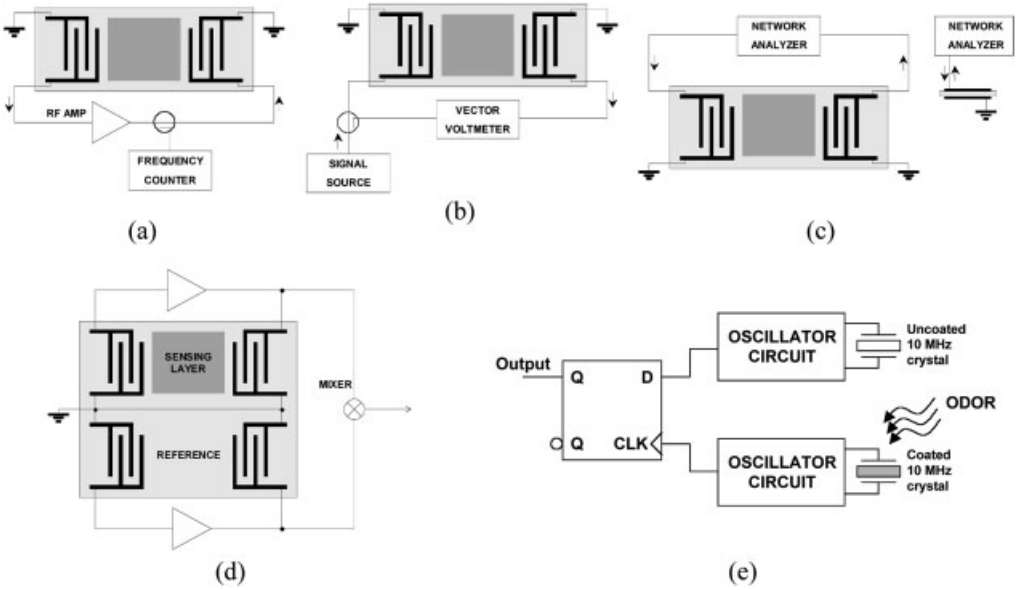

Fig. 5.4 Instrumentation configurations for acoustic wave sensors: (*a*) oscillator circuit, (*b*) impedance meter, and (*c*) network analyzer. (*d*) Dual delay SAW structure for temperature compensation [3, 11, 12]. (*e*) QMB sensor interface circuit [15]

Three instrumentation configurations, illustrated in Fig. 5.4, are commonly employed for acoustic wave sensors: oscillator circuits, vector voltmeters, and network analyzers. Oscillator circuits can be used for one-port (not shown in the figure) and two-port devices (Fig. 5.4a). The sensor is used as the resonant element in the feedback loop of an RF-amplifier circuit. Mass changes in the sensitive layer induce shifts in the resonance frequency, which are measured with a frequency counter. Oscillator circuits have several advantages, including low cost, relative simplicity, and excellent frequency stability [11]. However, these circuits generally provide information about wave velocity, and not amplitude, which may be necessary to monitor wave attenuations. A second configuration, shown in Fig. 5.4b, overcomes this limitation, providing both wave velocity and amplitude measurements in two-port devices. A signal generator is used to supply an RF voltage to the input transducer, and a vector voltmeter measures phase and amplitude changes at the output IDT relative to the input signal. Vector voltmeters are, however, relatively expensive pieces of laboratory equipment, and their phase measurements are 10–100 times less sensitive than frequency measurements with oscillator circuits. A third alternative, shown in Fig. 5.4c, is to use a network analyzer to perform a complete characterization of the device at multiple frequencies [11, 12].

To compensate for interferents (e.g., temperature, pressure, drift), SAW sensors are typically used in the dual configuration illustrated in Fig. 5.4d. One delay line is coated

with a sensing film that responds strongly to odors, and the second line is used as a reference to capture only interferent effects. Subtraction of the two signals yields a measurement that is, theoretically, independent of the common-mode interferents [13]. Fig. 5.4e shows a compact, low-power circuit for a QMB sensor [14, 15]. A 10 MHz sensor crystal is connected to an integrated oscillator whose output frequency decreases when odor molecules are absorbed into the crystal coating. The output of the sensor oscillator is compared to a reference oscillator with an uncoated 10 MHz crystal by means of a D flip-flop, which generates the difference frequency.

5.2.3 Field-Effect Gas Sensors

As described in Chapter 4, two configurations can be used in metal-insulator-semiconductor field-effect gas sensors: capacitor (MISCAP) and transistor (MISFET). The two structures depicted in Fig. 4.4 of Chapter 4 yield similar information, the differences being in the required measurement circuits[b]. In the case of MISCAP sensors, changes in the voltage-capacitance curve can be measured with a small AC-voltage (e.g., 1 MHz) superimposed on a DC-potential [16]. Changes in the $I_D - V_G$ curve of MISFET sensors, on the other hand, may be measured with constant-voltage [17] or constant-current circuits [18]. Figure 5.5 shows a conventional two-terminal arrangement

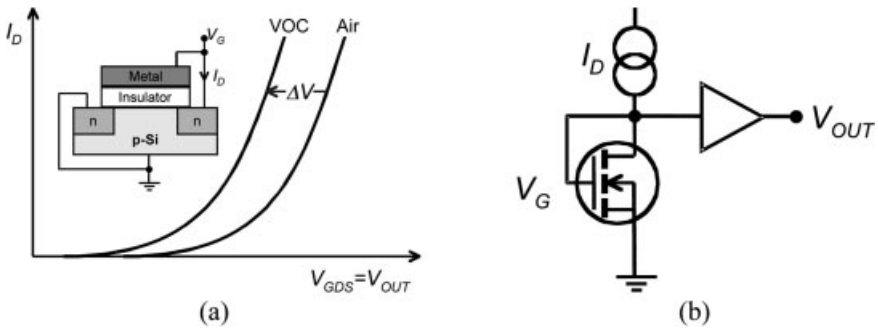

Fig. 5.5 MISFET gas sensors: (*a*) two-terminal configuration and (*b*) possible constant-current interface circuit [18, 19]

for an n-channel MISFET with a common gate-drain configuration, and a possible constant-current interface circuit. The shift in the $V_{GDS} - I_D$ curve upon exposure to volatile organic compunds is the change in the threshold voltage, which is in turn related to the shift in work function, surface states, and charge. A current source is used to inject a constant current into the drain, and the resulting voltage V_{GDS} is buffered (see Section 5.3.2) and sampled to create a time-resolved signal. Field-effect sensors operate at high temperatures (100 – 200 °C for Si substrates, up to 700 °C for

b) MISCAPs have a simpler structure and are, therefore, often used for exploratory work [16]

SiC) and, like metal-oxide chemoresistors, require temperature control circuits. Field-effect sensors also suffer from baseline drift, which can be compensated for by using differential configurations having an active gate FET and a passive reference FET [16].

5.2.4 Temperature Control

Metal-oxide gas sensors are commonly operated in the so-called isothermal mode, in which the temperature of the sensor is kept constant during exposure to odors[c]. The simplest and most widely used method for pseudo-isothermal operation consists of applying a constant voltage across the terminals of the resistive heater R_H, as shown in Fig. 5.6a. Temperature stability is achieved by using heater materials with a positive temperature coefficient[d] so that the thermoresistive effect serves as negative feedback [20]. This simple constant-voltage operation may be used when temperature stability is not critical.

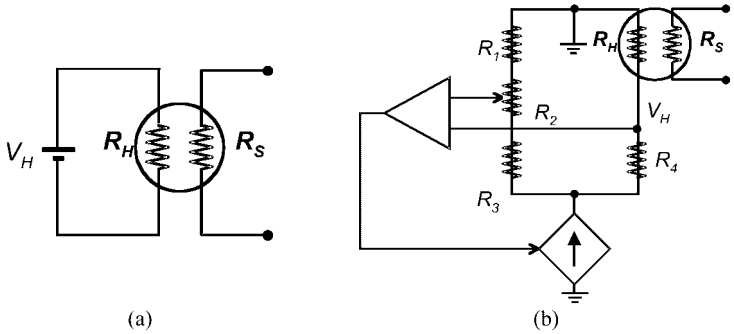

Fig. 5.6 (*a*) Constant heater voltage and (*b*) constant heater resistance circuits [20]

Improved stability (e.g., to gas-flow cooling effects) may be achieved by controlling the heater resistance rather than the heater voltage [21]. In constant-resistance operation, the sensor heater is placed in a Wheatstone bridge and compared against a reference potentiometer that determines a set-point resistance, as shown in Fig. 5.6b. Deviations from the set-point resistance result in a differential voltage across the bridge, which is used to control a current or voltage source. Capteur Ltd. implements constant-resistance control by using a FET operating as a voltage-controlled current source [22]. Constant resistance, however, requires heater materials with a reasonably high thermoresistive coefficient.

A third alternative consists of embedding a temperature sensor in the substrate [8], or using the heater as a temperature sensor [24, 25]. The latter method, however, also

c) If the sensor is normally operated at low temperature, it is then necessary to shift to a high temperature to burn off excess organic contaminants from the sensor surface [28].

d) The heater resistance R_H is a function of temperature T: $R_H = R_0(1 + \alpha T)$, where R_0 is the baseline resistance at zero degrees and α is the temperature coefficient. For positive α, the heater resistance increases with temperature.

requires a large positive thermoresistive coefficient, which is not the case for certain commercial metal-oxide sensors [26]. Sensor surface temperatures can also be measured with infrared thermometers, but these measurements have been shown to be rather inaccurate [26]. Additional temperature control strategies may be found in the literature [27].

5.3 Signal Conditioning

The electrical signals generated by sensor interface circuits are often not adequate for acquisition into a computer, and must be further processed by a number of analog signal conditioning circuits. The four basic roles of these circuits: buffering, amplification, filtering, and special functions, are surveyed in the following subsections along with a brief review of operational amplifiers.

5.3.1 Operational Amplifiers

Operational amplifiers (op-amps) are analog integrated circuits widely used to implement a variety of instrumentation circuits. Although a thorough coverage of op-amps is beyond the scope of this chapter, we provide a brief review that will allow the reader to analyze the circuits presented in the remaining sections of this chapter. An op-amp, shown in Fig. 5.7a, is essentially a high-gain amplifier that generates an output voltage $V_0 = G_{OL}V_d$ proportional to the difference voltage V_d between a noninverting (+) and an inverting input (−). The power necessary to perform the signal amplification ($G_{OL} \cong 10^4 - 10^6$) is derived from the supply voltages ($\pm V_\mathrm{S}$) and, therefore, the output voltage V_0 is constrained by $-V_S \leq V_0 \leq +V_S$. Op-amp circuits in this open-loop configuration are not practical since very small difference voltages V_d will drive the output voltage to saturation. In addition, the open-loop gain G_OL has a limited bandwidth (G_OL decays significantly with frequency), and is very sensitive to temperature and power supply fluctuations. For these reasons, op-amps circuits typically contain a feedback loop to control the gain, as shown in Fig. 5.7b.

A large number of these op-amp feedback circuits can be analyzed by assuming ideal op-amp characteristics, primarily (1) infinite open-loop gain and bandwidth $G_{OL}(f) = \infty$, (2) infinite input impedance $Z_{IN} = \infty$, and (3) zero output impedance $Z_{OUT} = 0$. The latter simply implies that loading effects are negligible, that is, $V_0 = V_\mathrm{OUT}$ in the equivalent op-amp circuit of Fig. 5.7a. These ideal characteristics lead to two 'golden rules' that are sufficient for analyzing many practical op-amp feedback circuits [23, 29]:

- Rule 1: Inputs stick together. Since the gain is infinite and V_OUT must be bounded, the feedback network will enforce an output V_OUT that cancels the differential voltage $V_\mathrm{d} = 0$.
- Rule 2: Inputs draw no current. This follows from the assumption that $Z_{IN} = \infty$.

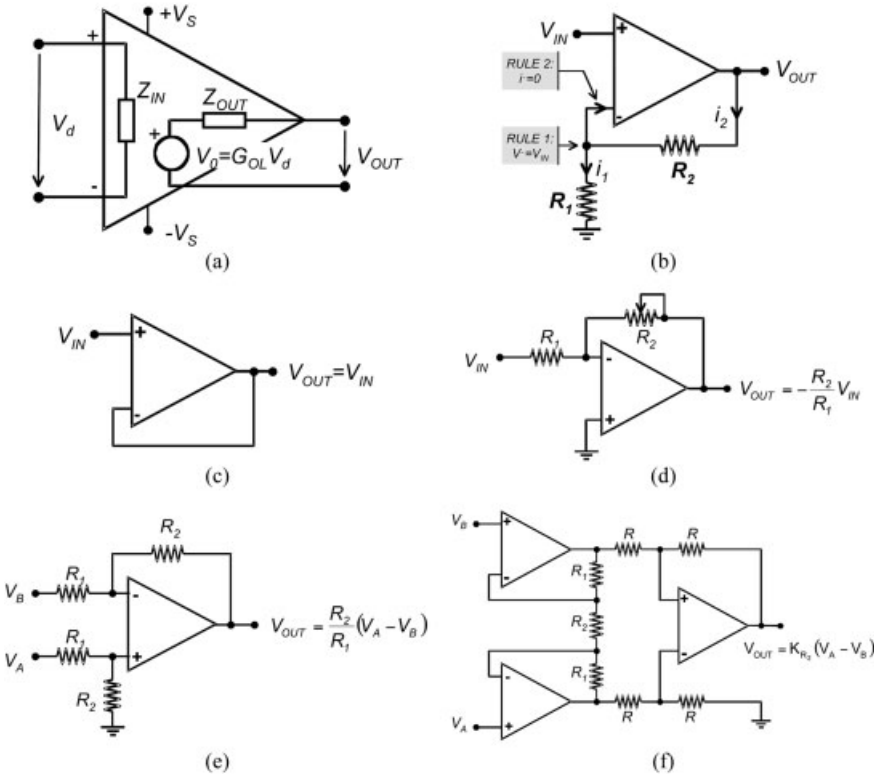

Fig. 5.7 (*a*) Op-amp simplified internal model and (*b*) analysis of feedback circuits. Amplifier circuits: (*c*) buffer, (*d*) inverting amplifier, (*e*) difference amplifier, and (*f*) instrumentation amplifier

To illustrate the use of these rules, we derive the transfer function of the circuit shown in Fig. 5.7b. From Rule 1 we can establish that the voltage at the noninverting input is equal to the input voltage V_{IN}. This allows us to express the current i_1 flowing through resistor R_1 as $i_1 = V_{IN}/R_1$. Since the noninverting input does not draw current (Rule 2), we infer that the current i_2 through resistor R_2 is equal to i_1. As a result, the voltage at the output becomes:

$$V_{OUT} = V_{IN} + R_2 i_2 = V_{IN} + R_2 \frac{V_{IN}}{R_1} = V_{IN}\left(\frac{R_2}{R_1} + 1\right) = V_{IN} G_{CL} \tag{7}$$

This circuit is known as a noninverting amplifier since it provides an amplification gain G_{CL} while preserving the phase (sign) of the input voltage V_{IN}.

5.3.2 Buffering

The first and simplest application of op-amps is buffering, which is required to isolate different electronic stages and avoid impedance-loading errors. An analog buffer can be implemented with the voltage-follower circuit shown in Fig. 5.7c. This circuit provides (assuming an ideal op-amp) infinite input impedance and zero output impedance.

5.3.3 Amplification

An amplification or gain stage is typically required to bring the signal of the interface circuits to a level that is suitable for the dynamic range of a subsequent analog-to-digital converter. Amplifier circuits can be broadly classified into single-ended or differential. A single-ended signal V_{IN}, such as the one from a voltage divider, can be amplified with the noninverting amplifier described earlier in Fig. 5.7b or its inverting counterpart shown in Fig. 5.7d, in which the feedback resistor has been replaced by a potentiometer to allow for manual adjustments of the gain.

In the case of Wheatstone bridge interface circuits, a differential amplifier stage, such as the one shown in Fig. 5.7e, may be used. This simple design, however, presents two basic drawbacks. First, the input impedance is significantly reduced since the R_1 resistors are in series with the input signals. Second, accurate matching of the resistor pairs ($R_{A1} = R_{B1}$) and ($R_{A2} = R_{B2}$) is required to ensure that the differential gains are similar and, therefore, provide good common-mode rejection. Due to these limitations, the so-called 'instrumentation amplifiers' are commonly used as difference stages. Fig. 5.7f shows a classical instrumentation amplifier design with three op-amps that can achieve high input impedance and common-mode rejection ratio without critical resistor matching [23]. The two op-amps at the input stage provide high differential gain and unity common-mode gain, whereas the second stage generates a single-ended output. Integrated instrumentation amplifiers are conveniently available from several manufacturers, with all components internal to the chip except for R_2, which can be connected externally to provide a programmable gain.

5.3.4 Filtering

Analog filters are used to remove unwanted frequency components from the sensor signals. Filters can be broadly grouped into four classes according to their frequency response [30, 31]: low-pass, high-pass, band-pass, and band-reject (Fig. 5.8). Low-pass filters allow frequencies below a cutoff frequency[e] to pass, while blocking frequencies

e) The cutoff frequency is defined as the frequency at which the gain is reduced by 3 dB (or a signal ratio of 0.707)

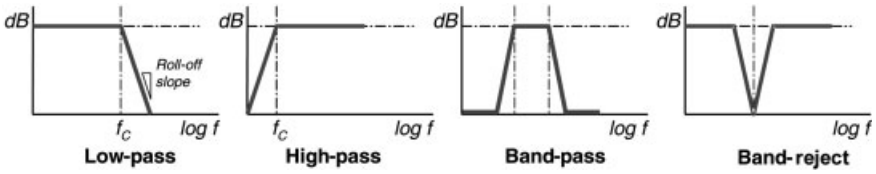

Fig. 5.8 Frequency response of analog filters

above the cutoff. High-pass filters perform the opposite function, passing only frequencies above a cutoff. Band-pass filters allow passage of frequencies within a band. Band-reject (or notch) filters allow passage of all frequencies except for those within a, typically narrow, band.

These analog filters can be implemented using passive or active circuits. Passive filters consist of networks of resistors, capacitors, and inductors, whereas active filters utilize active components (e.g., op-amps, transistors), in addition to passive devices, e.g. resistors and capacitors. Active filters are capable of implementing 'virtual' inductors by placing capacitors in the feedback loop, thus avoiding the bulk and nonlinearity of inductors[f]. Active filters are suitable for low frequency, small signals, and are preferred over passive filters because they can have gains greater than 0 dB. Conversely, active filters require a power supply and are limited by the bandwidth of the active element. Passive filters have the advantage of being low-noise. Fig. 5.9a shows a pas-

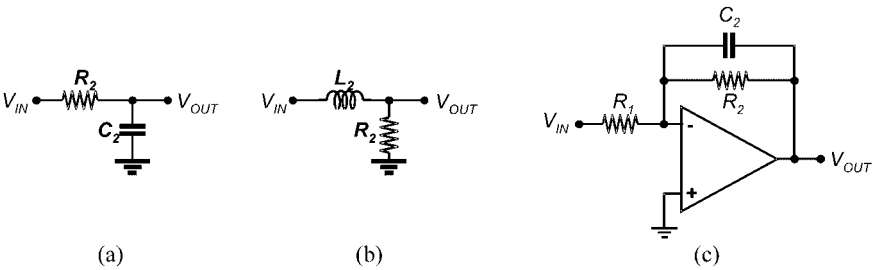

Fig. 5.9 Low-pass first order filters: (*a*, *b*) passive and (*c*) active

sive implementation of a first-order Butterworth (low-pass) filter, with a cut-off frequency $F_C = (2\pi R_2 C_2)^{-1}$ and a roll-off slope[g] of 20 dB/decade. Figure 5.9b shows an equivalent implementation with an inductor and a resistor. The active circuit shown in Fig. 5.9c also has a similar frequency response plus a static gain of R_2/R_1. Finally, integrated circuits with low-pass, high-pass, band-pass, and band-reject outputs are also available in a single package from several manufacturers. These circuits, known as state-variable filters, are provided with extensive design formulas and tables and can be easily configured using only external resistors.

f) Active filters could also use inductors, although they usually do not.

g) Steeper roll-offs may be achieved by cascading several filters in series.

5.3.5 Compensation

A number of special functions may be implemented with analog circuits to compensate for deficiencies, cross-sensitivities, and nonlinearities in the sensor response, and reduce the computational load of a subsequent digital signal processing stage. These circuits perform various functions including linearization, integration, differentiation, logarithmic and antilogarithmic conversion, peak-to-peak and phase detection, and temperature compensation [29]. We now introduce several interface circuits for chemoresistors that can be used to obtain linear resistance-voltage relationships. These circuits are presented here, rather than in Section 5.2.1 with the remaining interface circuits, because they require familiarity with op-amps and they perform a compensation function. Additional compensation circuits for concentration and temperature are reviewed in Section 5.3.5.2.

5.3.5.1 Linearization of Resistance Measurements

Among other shortcomings, voltage dividers have a nonlinear resistance-to-voltage transfer function. As a result, the sensitivity of the circuit is not constant over the dynamic range of the sensor. The resistance-to-voltage relationship can be easily linearized, however, by driving the sensing element at constant-voltage or constant-current. Figure 5.10a illustrates a constant-voltage measurement circuit that employs a virtual ground at the inverting input of the operational amplifier to apply a constant voltage V_{CC} across the sensor R_S [20]. Negative feedback through a load resistor generates an output that changes linearly with the sensor conductance G_S (the inverse of sensor resistance R_S):

$$V_{OUT} = -I_S R_L = -\frac{V_{CC}}{R_S} R_L = -V_{CC} R_L G_S \tag{8}$$

An additional advantage of this circuit is that the load resistor R_L can be chosen to provide different amplification gains.

Constant-current excitation is illustrated in Fig. 5.10b. The current I_S through the sensor is entirely determined by the load resistor since the voltage at the op-amp inverting input is constant and equal to V_{CC} [4]. The differential voltage across the sensor is then linearly proportional to the sensor resistance:

$$V_{OUT} = R_S I_S = R_S \frac{V_{CC}}{R_L} \tag{9}$$

A similar constant-current arrangement can be used to provide a linear resistance-voltage relationship in Wheatstone bridges, as shown in Fig. 5.10c [4]. The operational amplifier provides a virtual ground to the midpoint of the sensor arm, generating a constant current through the sensor:

$$I_S = \frac{V_{CC}}{R_0} \tag{10}$$

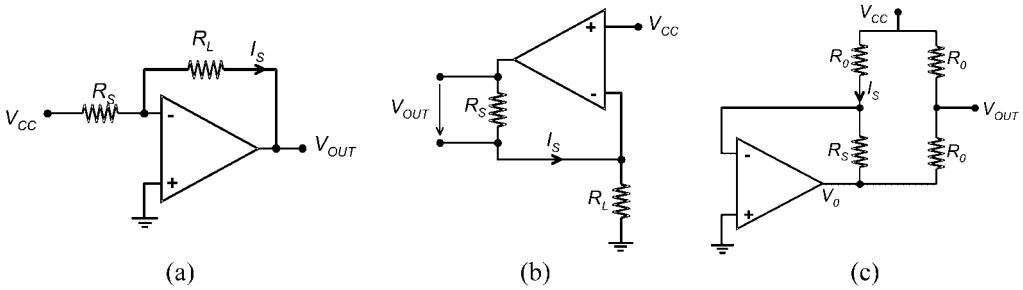

Fig. 5.10 Linearizing a voltage divider through constant-voltage (*a*) or constant-current (*b*) measurements. Linearization of a Wheatstone bridge with a constant-current arrangement (*c*)

The voltage at the output of the op-amp is then proportional to the sensor resistance:

$$V_0 = -R_S I_S - R_S \frac{V_{CC}}{R_0} \tag{11}$$

and the output of the circuit becomes:

$$V_{Out} = \frac{1}{2} V_{CC}\left(1 - \frac{R_S}{R_0}\right) = \frac{1}{2} V_{CC}\left(1 - \frac{R_0(1-a)}{R_0}\right) = \frac{1}{2} V_{CC} a \tag{12}$$

5.3.5.2 Miscellaneous Functions

A number of miscellaneous compensation functions may be performed with analog circuits. Figure 5.11a shows a logarithmic amplifier that may be used to compensate for the power-law concentration-resistance relationship $R \propto [C]^{-\beta}$ of metal-oxide chemoresistors [32] and provide an output voltage proportional to the log concentration log[C] of the analyte[h]. Figure 5.11b illustrates a circuit that is employed in commercial

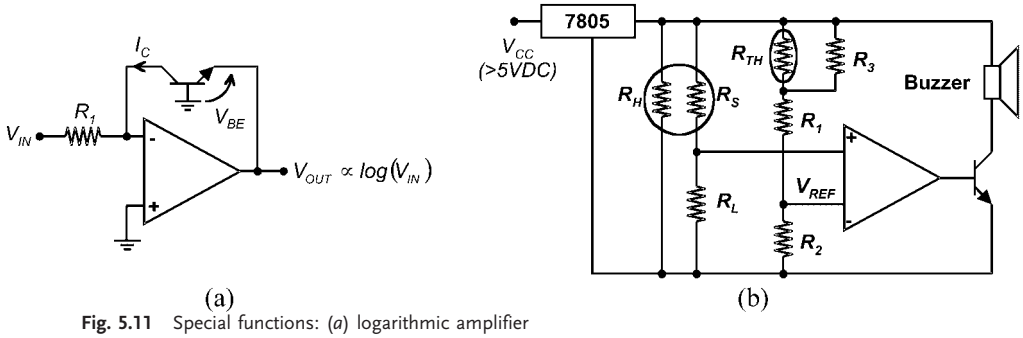

Fig. 5.11 Special functions: (*a*) logarithmic amplifier and (*b*) temperature compensation [1]

h) The relationship $V_{BE} \propto \log(I_C)$ may be used to derive the logarithmic transfer function. This simple circuit, however, requires additional compensation for oscillations and ambient temperature [29].

gas alarm circuits to compensate for temperature [1, 2]. The circuit includes a thermistor R_{TH} (temperature dependent resistor) that adapts the alarm reference voltage V_{REF} according to ambient temperature. The schematic in Fig. 5.11b uses a voltage regulator (7805) to provide a stable 5 V DC supply voltage to the heater and the voltage divider. Finally, the output of the comparator is current-boosted with an NPN transistor in order to drive an alarm.

5.4 Signal Preprocessing

Following an appropriate conditioning stage, the sensor array signals are digitized and either processed online or stored for future analysis. Due to space constraints, the reader is referred to the existing literature [30, 33] for a review of data acquisition for sensor systems (e.g., sample/hold, anti-aliasing, and analog-to-digital conversion). It is important to mention, however, that in order to avoid aliasing effects, the sampling rate during data acquisition should be at least twice the highest frequency in the sensor response. This is known as the Nyquist sampling theorem [34].

With this in mind, we focus our attention on signal preprocessing, the first computational stage after the sensor array data has been sampled and stored into computer memory. The goal of signal preprocessing is to extract relevant information from the sensor responses and prepare the data for multivariate pattern analysis (covered in Chapter 6). The choice of signal preprocessing is critical and can have a significant impact on the performance of subsequent modules in the pattern analysis system [35]. Although signal preprocessing is somewhat dependent on the underlying sensor technology, three general stages can be identified [36]: baseline manipulation, compression, and normalization.

5.4.1 Baseline Manipulation

The first stage of preprocessing consists of manipulating the sensor response with respect to its baseline (e.g., response to a reference analyte) for the purposes of drift compensation, contrast enhancement and scaling. Considering the dynamic response of the sensor $x_S(t)$ shown in Fig. 5.12a, three techniques are commonly employed [3]:

- Differential: the baseline $x_S(0)$ is subtracted from the sensor response. As a result, any additive noise or drift δ_A that may be present in the sensor signal is effectively removed from the preprocessed response $y_S(t)$:

$$y_S(t) = (x_S(t) + \delta_A) - (x_S(0) + \delta_A) = x_S(t) - x_S(0) \tag{13}$$

- Relative: the sensor response is divided by the baseline. Relative measurements eliminate the effect of multiplicative drift δ_M and provide a dimensionless response $y_S(t)$:

$$y_S(t) = \frac{x_S(t)(1+\delta_M)}{x_S(0)(1+\delta_M)} = \frac{x_S(t)}{x_S(0)} \tag{14}$$

- Fractional: the baseline is subtracted and then divided from the sensor response. Fractional measurements are not only dimensionless but also normalized since the resulting response $y_S(t)$ is a per-unit change with respect to the baseline, which compensates for sensors that have intrinsically large (or small) response levels:

$$y_S(t) = \frac{x_S(t) - x_S(0)}{x_S(0)} \tag{15}$$

The choice of baseline manipulation technique and response parameter $x_S(t)$ (e.g., resistance, conductance, frequency) is highly dependent on the sensor technology and the particular application, but a few general guidelines can be extracted from

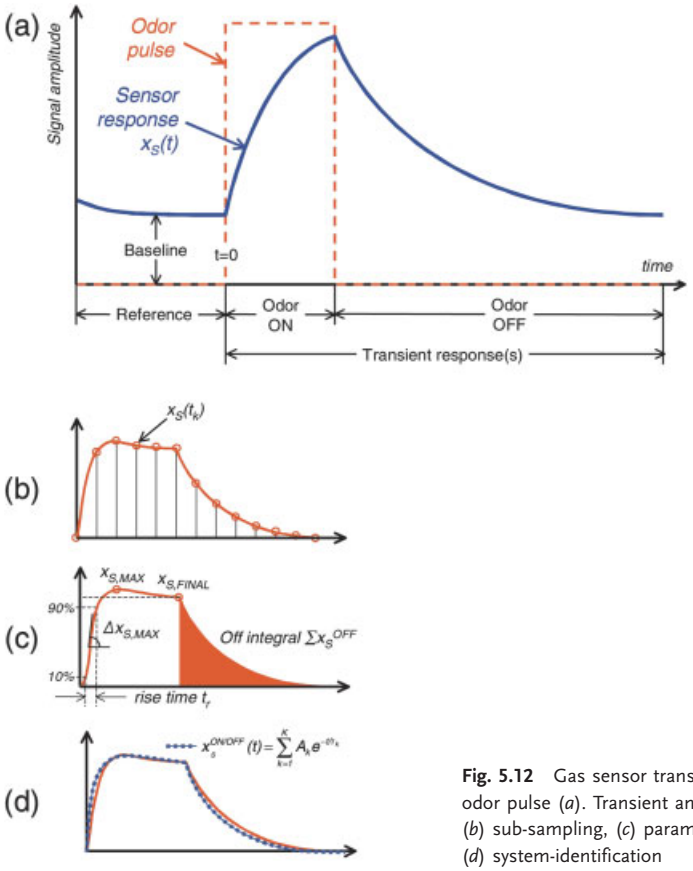

Fig. 5.12 Gas sensor transient response to an odor pulse (*a*). Transient analysis approaches: (*b*) sub-sampling, (*c*) parameter-extraction, and (*d*) system-identification

the literature. Gardner et al. [37, 38] have shown that the fractional change in conductance $y_S(t) = (G_S(t) - G_S(0)/G_S(0)$ provides the best pattern-recognition performance for (*n*-type) MOS chemoresistors, compensating for temperature cross-sensitivity and nonlinearities in the concentration dependence [39]. Fractional methods for MOS chemoresistors are also widely used [40, 41]. In the case of conducting polymer chemoresistors, fractional changes in resistance are commonly employed, both in research prototypes and in commercial instruments [42, 43]. For piezo-electric oscillators, where the response $x_S(t)$ being monitored is a frequency, differential measurements with respect to a reference analyte (and/or an uncoated reference sensor) are commonly used [12, 44]. Differential measurements are also widely used for MOSFETs [45, 46], where the response $x_S(t)$ is a voltage shift in the I(V) curve as described in Section 5.2.3. Finally, a number of variations of these three basic baseline-manipulation techniques have been proposed in the literature, including data-driven procedures to optimize the baseline-manipulation stage for specific applications [35, 36, 47].

5.4.2 Compression

The second stage in preprocessing is aimed at compressing the sensor-array response down to a few descriptors to form a feature vector or fingerprint. In most cases this is performed by extracting a single parameter (e.g., steady-state, final, or maximum response) from each sensor, disregarding the initial transient response, which may be affected by the fluid dynamics of the odor delivery system (covered in Chapter 3). However, with careful instrument design and sampling procedures, transient analysis can significantly improve the performance of gas sensor arrays:

- Improved selectivity. The dynamic response to an odor exposure (and the subsequent odor recovery) carries a wealth of odor-discriminatory information that cannot always be captured with a single parameter. In some situations, transient parameters have also been reported to exhibit better repeatability than static descriptors [48–50]. Therefore, sensor transients can be used as dynamic fingerprints to improve selectivity by pattern-recognition means.
- Reduced acquisition time. The duration of the acquisition cycles can be significantly shortened if the initial sensor transients contain sufficient discriminatory information, avoiding the lengthy acquisition times required to reach steady state [51]. As a consequence, the sensors also require less time to recover their baseline, a process that can be particularly slow when the target odors have high concentrations.
- Increased sensor lifetime. By reducing the duration of the odor pulse and, therefore minimizing irreversible binding, the lifetime of the sensors can also be increased.

For these reasons, transient analysis has received much attention in recent years. According to the procedure employed to generate the dynamic fingerprint, transient compression methods can be broadly grouped into three classes:

- Sub-sampling methods: As depicted in Fig. 5.12b, these methods exploit dynamic information by sampling the sensor transient response (and/or its derivatives) at different times during the odor exposure and/or odor recovery phase [36, 49, 52, 53].
- Parameter-extraction methods: These methods compress the transient response using a number of descriptors, such as rise times, maximum/minimum responses and slopes, and curve integrals. [48, 54 – 56].
- System-identification methods: These methods fit a theoretical model (e.g., multi-exponential, auto-regressive) to the experimental transients and use the model parameters as features [55, 57, 58].

Exponential curve-fitting methods can result in nearly lossless compression of the sensor transients, but are computationally intensive [57, 59]. For these reasons, sub-sampling and parameter-extraction methods are more commonly employed. A final word of caution regarding the use of transient information: a large number of dynamic parameters will require an exponentially increasing number of training examples in order to prevent the pattern recognition system from over-fitting the data. Alternatively, one may use resampling techniques (e.g., cross-validation, bootstrap) or regularization (e.g., shrinkage, weight decay) to control the complexity of the model. Further details on small-database considerations and dynamic pattern-recognition methods may be found in Chapter 12 of this Handbook.

5.4.3 Normalization

Normalization constitutes the final stage of digital preprocessing prior to multivariate pattern analysis. Normalization techniques can be broadly grouped in two classes: local and global methods. Local methods operate across the sensor array on each individual "sniff" in order to compensate for sample-to-sample variations caused by analyte concentration and sensor drift, among others. Global methods, on the other hand, operate across the entire database for a single sensor (e.g., the complete history of each sensor), and are generally employed to compensate for differences in sensor scaling. In what follows, we will denote by $x_S^{(k}$ the response of sensor 's' to the k-th example in the database.

5.4.3.1 Local Methods

The most widely used local method is vector normalization, in which the feature vector of each individual 'sniff' is divided by its norm and, as a result, forced to lie on a hypersphere of unit radius, as shown in Fig. 5.13d,e:

$$y_S^{(k} = \frac{x_S^{(k}}{\sqrt{\sum_S (x_S^{(k})^2}} \tag{16}$$

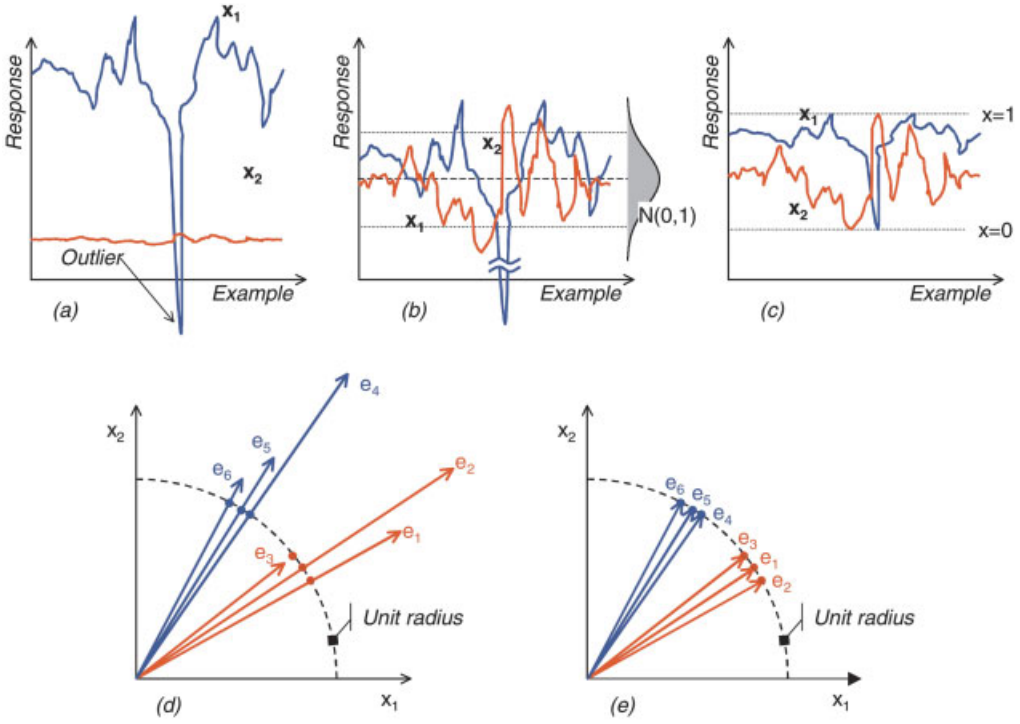

Fig. 5.13 Normalization procedures: (a,d) raw data, (*b*) sensor autoscaling, (*c*) sensor normalization and (*e*) vector normalization

Vector normalization can be employed to compensate for differences in concentration between samples. Assuming the power-law relationship $x_{s,a}^{(k} = \alpha_{s,a}[C_a^{(k}]^{\beta}$ of metal-oxide chemoresistors [32], where $x_{s,a}^{(k}$ is the response of sensor 's' to the k-th sample of odor 'a', $\alpha_{s,a}$ is the sensitivity of sensor 's' to odor 'a', and $[C_a^{(k}]$ is the concentration of the k-th sample of odor 'a', then:

$$y_{s,a}^{(k} = \frac{x_{s,a}^{(k}}{\sqrt{\sum_s \left(x_{s,a}^{(k}\right)^2}} = \frac{\alpha_{s,a}\left[C_a^{(k}\right]^{\beta}}{\sqrt{\sum_s \left(\alpha_{s,a}\left[C_a^{(k}\right]^{\beta}\right)^2}} = \frac{\alpha_{s,a}}{\sqrt{\sum_s \left(\alpha_{s,a}\right)^2}} \tag{17}$$

To the extent that these simplifying assumptions hold, vector normalization can therefore be used to compensate for sample-to-sample variations in concentration. In this context, vector normalization can be applied in situations when each odor has a unique concentration, but discrimination is to be performed on the basis of odor quality (e.g., the direction of the response vector $\overrightarrow{x}_a^{(k}$) rather than odor intensity (e.g., the magnitude of $\overrightarrow{x}_a^{(k}$). Conversely, this method should not be used when the vector amplitude is known to carry relevant information.

5.4.3.2 Global Methods

Two global procedures are commonly employed in electronic nose systems:

- Sensor autoscaling, in which the distribution of values for each sensor across the entire database is set to have zero mean and unit standard deviation:

$$y_s^{(k} = \frac{x_s^{(k} - mean[x_s]}{std[x_s]} \tag{18}$$

- Sensor normalization, in which the range of values for each individual sensor is set to [0,1]. This is simply done by subtracting the minimum and dividing by the range of the sensor across the entire database:

$$y_s^{(k} = \frac{x_s^{(k} - \min_{\forall k}[x_s^{(k}]}{\max_{\forall k}[x_s^{(k}] - \min_{\forall k}[x_s^{(k}]} \tag{19}$$

Global methods are typically used to ensure that sensor magnitudes are comparable, preventing subsequent pattern-recognition procedures from being overwhelmed by sensors with arbitrarily large values. For instance, nearest-neighbors procedures are extremely sensitive to feature weighting, and multilayer perceptrons can saturate their sigmoidal activation functions for large inputs. Sensor normalization makes full use of the input dynamic range but, as illustrated in Fig. 5.13a,c, is very sensitive to outliers since the range is determined by data outliers. Autoscaling, on the other hand, cannot provide tight bounds for the input range but is robust to outliers. However, it must be noted that both techniques can amplify noise since all the sensors (particularly those which may not carry information) are weighted equally.

Logarithm metrics have also been used to compensate for highly nonlinear concentration effects [41]. It is also worth mentioning the Box-Cox transform [60], which could be employed to compensate for nonlinearities, as well as compress the dynamic range of the sensors:

$$y_s^{(k} = \begin{cases} \frac{(x_s^{(k})^{\lambda} - 1}{\lambda} & \lambda \neq 0 \\ \ln\left(x_s^{(k}\right) & \lambda = 0 \end{cases} \tag{20}$$

5.5 Noise in Sensors and Circuits

Noise is generally considered to be any unwanted effect that obscures the detection or measurement of the desired signal. As shown in Fig. 5.14a, noise can arise at various stages in the measurement process, including the quantity under measurement itself, the sensors, the analog processing system, the data acquisition stage and the digital signal processing system. Among these, noise in the early measurement stages is clearly most harmful as it propagates and can be potentially amplified through the

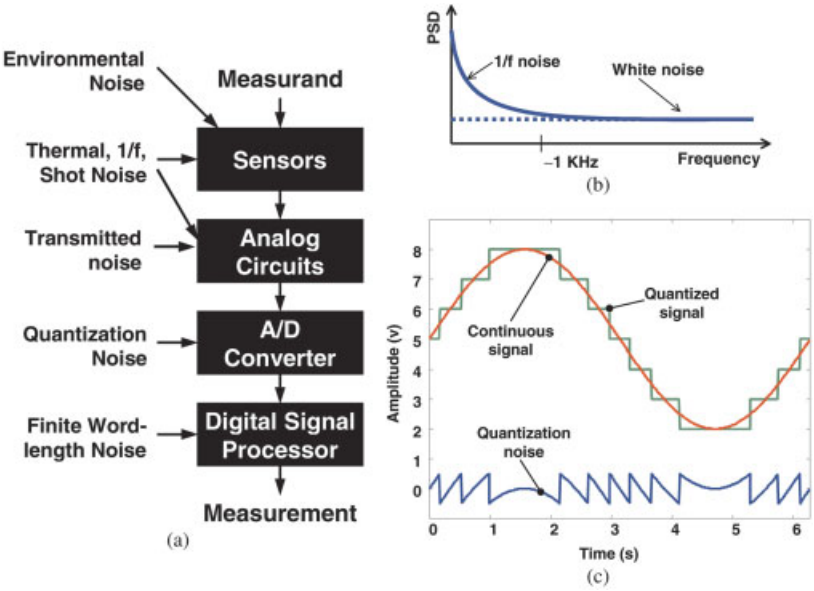

Fig. 5.14 (*a*) Sources of noise in sensor systems. (*b*) Power spectral density of white and $1/f$ noise. (*c*) Quantization noise in A/D conversion

subsequent stages in the signal pathway [61]. Several noise sources, such as thermal and shot noise, are inherent to the underlying physics of the sensors or electronic components and are, therefore, irreducible. Other types of noise, conversely, are originated from processes that could be avoided, and include $1/f$ noise, transmission and quantization noise.

Thermal noise, also known as Johnson or Nyquist noise, arises in any medium that dissipates energy, such as a conductor. This means that even a simple resistor is a noise source. The open-circuit noise voltage generated by a resistance R is $V_{noise} = \sqrt{4kTR\Delta f}$, where k is Boltzman's constant, T is the absolute temperature (Kelvins), and Δf is the bandwidth (Hz) over which the measurement is made [23]. Therefore, the larger the resistance, the more noise it can introduce. Thermal noise has a flat power spectral density (PSD), and is oftentimes called white noise in analogy to white light, which has a flat distribution of all frequencies in the visible spectrum. In addition, the amplitude distribution of thermal noise is Gaussian [23].

Shot or Schottky noise arises from the random fluctuations in the number of charge carriers (electrons and holes) that cross a potential barrier in the charge flow, and is typical of p-n junctions in diodes and transistors. The shot-noise RMS current fluctuation is $I_{noise} = \sqrt{2qI_{DC}\Delta f}$, where q is the electron charge, I_{DC} is the average current through the barrier, and Δf is the bandwidth. Shot noise is also white and Gaussian [4].

$1/f$ (read 'one-over-f') or flicker noise is considered to arise from imperfections in the manufacturing process of electronic components. As the name indicates, $1/f$ noise has

a PSD that is inversely proportional to frequency. For this reason it is also known as low-frequency or pink noise (red is at the low side of the visible spectrum). It is also referred to as excess noise because it appears in addition to white noise, as illustrated in Fig. 5.14b. $1/f$ noise is most pronounced at frequencies below 100 Hz, where many sensors operate, and becomes barely noticeable at frequencies above a few hundred KHz where white noise dominates. In contrast with thermal noise, which equally affects a cheap carbon resistor or the most carefully made resistor, $1/f$ noise can be reduced by using good quality metal film or wire-wound resistors at the early stages of sensor interface circuits [23].

Noise can also be transmitted from interferences such as fluctuations in the DC power supply, 50 – 60 Hz pickup, changes in ambient temperature, capacitive or inductive couplings, and ground loops. A careful layout and construction of the electronics, with proper shielding and grounding, must be used to reduce electromagnetic interference noise to acceptable levels [23]. In addition, differential measurements, such as the ones in Fig. 5.4d,e, can be employed to compensate for noise effects that are additive in nature. Multiplicative effects, on the other hand, can be reduced by means of ratiometric measurement techniques [5]. Analog filtering (Section 5.3.4) and digital signal preprocessing (Section 5.4) can also be employed to further reduce noise. For instance, differentiation can be used to reduce low-frequency noise (e.g., drift) at the expense of amplifying high-frequency components. Conversely, integration or averaging reduces high-frequency noise while amplifying low-frequency components.

As mentioned earlier, noise can also arise in the latter stages of the signal pathway, primarily during analog-to-digital conversion, when the continuous sensor signals are converted into a discrete subset of values and stored in computer memory. This process introduces nonlinear quantization errors that can be treated as an additional noise source, as depicted in Fig. 5.14c. Quantization noise must be controlled by selecting an appropriate gain in the signal conditioning circuits to fully utilize the dynamic range of the analog-to-digital converter, and by employing differential measurements to remove uninformative baseline offsets in the sensor response [62]. Limitations in machine precision and fixed-point arithmetic can also introduce digital noise in the signal pathway. For a systematic treatment of quantization and finite word-length noise, the reader is referred to the literature [34].

Finally, it is important to notice that the inherent drift and poor repeatability of the sensor responses can sometimes be significantly larger than most of the other noise sources described in this section, effectively limiting the sensitivity of electronic nose systems. As proposed previously [61], the global effect of all these noise sources can be combined into a single parameter called the noise-equivalent concentration, which indicates the gas concentration that results in a unit signal-to-noise ratio.

5.6 Outlook

From their original conception as arrays of homogeneous gas sensors with overlapping selectivities, electronic-nose systems, including those commercially available, are slowly evolving towards hybrid arrays that take advantage of several sensor technologies [63]. The use of sample preconditioning such as thermal-desorption units or chromatographic columns, is also becoming increasingly popular as the means to increase the sensitivity and selectivity of the instrument [64–66]. An additional trend in electronic-nose systems has become the measurement of multiple parameters from the same sensing membrane [67]. We focus our attention on the latter, since the use of hybrid systems does not introduce conceptual problems other than the integration of the various sensor technologies into a single package, and sample preconditioning methods are covered in Chapter 3 of this Handbook. Multiparameter sensing approaches can be broadly grouped in three categories:

- Similar sensing layer but different transduction principles: these systems extract multiple physical parameters from the same sensing layer, such as work function and conductance on MOS sensors, or resistance and mass changes in conducting polymer sensors.
- Similar sensing layer and transduction principle but different operating modes: in this case, the selectivity of the sensor is modified by modulating the operating conditions, such as temperature cycling in MOS sensors or AC impedance spectroscopy in MOS or conducting polymer sensors.
- Similar sensing layer, transduction principle, and operating modes but different features: A third possibility is to extract multiple parameters from the sensor transient response.

In this section, we review a multiparameter technique for metal-oxide sensors that has received much attention in recent years: temperature modulation. AC impedance spectroscopy and transient analysis, which can also been used as multiparameter approaches to improve the selectivity of gas sensors, were covered in Sections 5.2.1.3 and 5.4.2, respectively. For additional material on multiparameter sensor systems the reader is referred to the authoritative review of Weimar and Göpel [67].

5.6.1 Temperature Modulation

The selectivity of metal-oxide sensors is greatly influenced by the operating temperature of the device, since the reaction rates for different volatile compounds and the stability of adsorbed oxygen species are a function of surface temperature [68]. This temperature-selectivity dependence can be utilized to improve the performance of MOS sensors. Rather than maintaining a constant operating point, as described in Section 5.2.4, the temperature of the sensor may be cycled during exposure to an odor

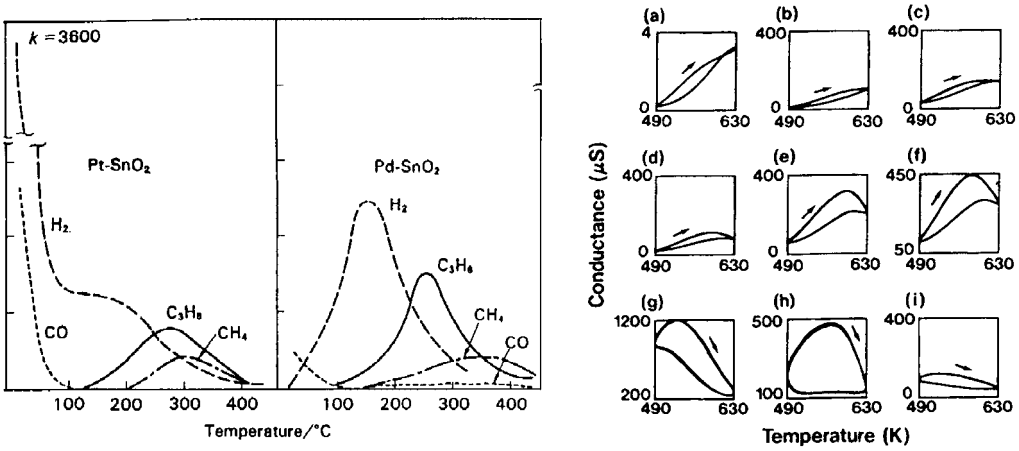

Fig. 5.15 Left: Sensitivity-temperature profile for Pt- and Pd-doped tin-oxide sensors [70]. Right: conductance-temperature response of a tin-oxide gas sensor in (*a*) air, (*b*) methane, (*c*) ethane, (*d*) propane, (*e*) *n*-butane, (*f*) isobutene, (*g*) ethylene, (*h*) propylene, and (*i*) carbon monoxide [71]

to obtain a multivariate dynamic signature. Figure 5.15a illustrates the sensitivity profiles of several doped tin-oxide gas sensors at different temperatures when exposed to various analytes. If maximum sensitivity to a particular analyte, say C_3H_8, were needed, a constant temperature of 250 °C for the Pd-doped sensor would then be most suitable. For machine olfaction applications, however, where the analyte detection range is broader, it would be advantageous to capture the response of the sensor over the entire temperature range. Figure 5.15b shows the conductance-temperature dynamic response to various analytes when a sinusoidal voltage (2 – 5 V, 0.04 Hz) is applied to the heater of a commercial SnO_2 sensor (Figaro TGS813). It can be observed that not only the magnitude of the conductance but also the shape of the dynamic response is unique to each analyte. An excellent survey of temperature modulation in semiconductor gas sensing may be found in [69].

5.7 Conclusions

This chapter has presented the hardware and software components that constitute the interface between chemical sensor arrays and pattern analysis techniques, the two critical building blocks in odor-sensing systems. We have surveyed a number of interface circuits that can be used to generate electrical signals for the most popular gas sensing technologies: chemoresistive, acoustic wave, and field effect sensors. Analog signal conditioning of the resulting electrical signals has also been outlined, including a gentle review of operational amplifiers. Various approaches for controlling the

operating temperature of metal-oxide sensors have also been presented. Finally, preprocessing algorithms to prepare sensor-array data for multivariate pattern analysis have been described. Although often overlooked, careful selection of sensor interface circuits, signal conditioning, and preprocessing is critical for achieving optimal performance in odor-sensing systems.

5.8 Acknowledgements

This work was partially supported by the award NSF/CAREER 9984426. The authors are grateful to J. W. Gardner and T. C. Pearce for helpful suggestions during the review process of this manuscript.

References

1 Figaro, *General Information for TGS Sensors*, Figaro Engineering, Inc., Osaka, Japan, **1996**.

2 FIS, *Products Review*, FIS Inc., Osaka, Japan, **1998**.

3 J. W. Gardner, P. N. Bartlett. *Electronic Noses, Principles and Applications*, Oxford University Press, Oxford, UK, **1999**.

4 R. Pallas-Areny, J. G. Webster. *Sensors and Signal Conditioning*, 2nd Edition, Wiley, New York, **2001**.

5 J. Fraden. *Handbook of Modern Sensors. Physics, Designs and Applications*, 2nd Edition, American Institute of Physics, Woodbury, New York, **1997**.

6 W. Göpel, K. D. Schierbaum. *Sens. Actuators B*, **1995**, 26–27, 1–12.

7 U. Hoefer, K. Steiner, E. Wagner. *Sens. Actuators B*, **1995**, 26–27, 59–63.

8 U. Weimar, W. Göpel. *Sens. Actuators B*, **1995**, 26–27, 13–18.

9 G. Sberveglieri. *Sens. Actuators B*, **1995**, 23, 103–109.

10 M. E. H. Amrani, K.C. Persaud, P. A. Payne. *Meas. Sci. Technol.*, **1995**, 6(10), 1500–1507.

11 J. W. Grate, G. C. Frye. In *Sensors Update Vol. 2*, (Eds.: H. Baltes, W. Göpel and J. Hesse), VCH, Weinheim, **1996**, Chapter 2.

12 J. W. Grate, S. J., Martin, R. M. White. Anal. Chem., **1993**, 65(21), 940–948.

13 D. S. Ballantine, R. M. White, S. I. Martin, A. J. Ricco, E. T. Zellers, G.C. Frye, H. Wohltjen. *Acoustic Wave Sensors. Theory, Design and Physico-Chemical Applications*, Academic Press, San Diego, CA, **1997**.

14 A. Russell. *Odour detection by mobile robots*, World Scientific, Singapore, **1999**.

15 R. A. Russell, L. Kleeman, S. Kennedy. *Proceedings of the 2000 Australian Conference on Robotics and Automation*, Melbourne, Aug. 30-Sept. 1, **2000**, 87–92.

16 A. Spetz, F. Winquist, H. Sundgren, I. Lundstrom. 1992, in *Gas Sensors* (Ed.: G. Sverveglieri), Kluwer Academic Publishers, **1992**, 219–279.

17 J. V. Hatfield, J. A. Covington, J. W. Gardner. *Sens. Actuators B*, **2000**, 65(1–3), 253–256.

18 I. Lundstrom, E. Hedborg, A. Spetz, H. Sundgren, F. Winquist. In *Sensors and Sensory Systems for an Electronic Nose*, (Eds.: J. W. Gardner, P. N. Bartlett), Kluwer Academic Publishers, Dordrecht, **1992**, 303–319.

19 R. C. C. Li, P. C. H. Chan, P. W. Cheung. *Sens. Actuators B*, **1995**, 28(3), 233–242.

20 K. Ikohura, J. Watson. *The Stannic Oxide Gas Sensor, Principles and Applications*, CRC Press, Boca Raton, FL., **1994**.

21 M. Benammar, W. C. Maskell. *J. Phys. E: Sci. Instrum.*, **1989**, 22, 933–936.

22 P. McGeeghin, P. T. Moseley, D. E. Williams. *Sensor Review*, **1994**, 14(1), 13–19.

23 P. Horowitz, W. Hill. *The art of electronics*, Cambridge University Press, Cambridge, UK, **1989**.

24 A. Heilig, N. Barsan, U. Weimar, W. Göpel. *Sens. Actuators B*, **1999**, 58(1–3), 302–309.
25 S. Jonda, M. Fleischer, H. Meixner. *Sens. Actuators B*, **1996**, 34(1–3), 396–400.
26 A. P. Lee, B. J. Reedy. *Sens. Actuators B*, **2000**, 69(1–2), pp. 37–45.
27 P. Mielle. *Sens. Actuators B*, **1996**, 34(1–3), 533–538.
28 W. M. Sears, K. Colbow, F. Consadori. *Sens. Actuators*, **1989**, 19, 333–349.
29 J. J. Carr. *Designer's Handbook of Instrumentation and Control Circuits*, Academic Press, San Diego, CA, **1991**.
30 H. R. Taylor. *Data Acquisition for Sensor Systems*, Chapman and Hall, London, UK, **1997**.
31 D. C. Ramsay. *Principles of Engineering Instrumentation*, Arnold, London, UK, **1996**.
32 P. K. Clifford, D. T. Tuma. *Sens. Actuators*, **1982**, 3, 233–254.
33 J. Brignell, N. White. *Intelligent sensor systems*, Institute of Physics Publishing, Bristol, UK, **1996**.
34 C. L. Phillips, H. T. Nagle. *Digital Control System Analysis and Design*, Prentice Hall, Englewood Cliffs, New Jersey, **1995**.
35 J. W. Gardner, M. Craven, C. Dow, E. L. Hines. *Meas. Sci. Technol.*, **1998**, 9, 120–127.
36 R. Gutierrez-Osuna, H. T. Nagle. *IEEE Trans. Sys. Man Cyber. B*, **1999**, 29(5), 626–632.
37 J. W. Gardner. *Sens. Actuators B*, **1991**, 4, 109–115.
38 J. W. Gardner, E. L. Hines, H. C. Tang. *Sens. Actuators B*, **1992**, 9, 9–15.
39 J. W. Gardner, P. N. Bartlett. *Sens. Actuators B*, **1994**, 18–19, 211–220.
40 G. Horner, C. Hierold. *Sens. Actuators B*, **1990**, 2, 173–184.
41 H. Abe, T. Yoshimura, S. Kanaya, Y. Takahashi, Y. Miyashita, S.-I. Sasaki. *Anal. Chim. Acta*, **1987**, 194, 1–9.
42 K.C. Persaud, S.M. Khaffaf, J.S. Payne, A.M. Pisanelli, D.-H. Lee, H.-G. Byun. *Sens. Actuators B*, **1996**, 36(1–3), 267–273.
43 E. J. Severin, B. J. Doleman, N. S. Lewis. *Anal. Chem.*, **2000**, 72(4), 658–668.
44 A. Hierlemann, U. Weimar, G. Kraus, M. Schweizer-Berberich, W. Göpel. *Sens. Actuators B*, **1995**, 26(1–3), 126–134.
45 H. Sundgren, F. Winquist, I. Lukkari, I. Lundstrom. *Meas. Sci. Technol.*, **1991**, 2(5), 464–469.
46 N. Paulsson, F. Winquist. *Forensic Sci. Int.*, **1999**, 105(2), 95–114.
47 T.C. Pearce, J. W. Gardner. *The Analyst*, **1998**, 123, 2057–2066.
48 E. Llobet, J. Brezmes, X. Vilanova, X. Correig, J.E. Sueiras. *Sens. Actuators B*, **1997**, 41(1–3), 13–21.
49 S. Roussel, G. Forsberg, V. Steinmetz, P. Grenier, V. Bellon-aurel. *J. Food Eng.*, **1998**, 37, 207–22.
50 B.W. Saunders, D.V. Thiel, A. Mackay-Sim. *The Analyst*, **1995**, 120, 1013–1018.
51 F. Sarry, M. Lumbreras. *Sens. Actuators B*, **2000**, 67, 258–264.
52 J. White, J. S. Kauer, T. A. Dickinson, D. R. Walt. *Anal. Chem.*, **1996**, 68(13), 2191–2202.
53 B. G. Kermani, S. S. Schiffman, H. T. Nagle. *IEEE Trans. Instrum. Meas.*, **1998**, 47(3), 728–741.
54 D. M. Wilson, S. P. DeWeerth. *Sens. Actuators B*, **1995**, 28, 123–128.
55 T. Eklov, P. Martensson, I. Lundstrom. *Anal. Chim. Acta*, **1997**, 353, 291–300.
56 T. D. Gibson, O. Prosser, J. N. Hulbert, R. W. Marshall, P. Corcoran, P. Lowery, E. A. Ruck-Keene, S. Heron. *Sens. Actuators B*, **1997**, 44(1–3), 413–422.
57 R. Gutierrez-Osuna, H. T. Nagle, S. S. Schiffman. *Sens. Actuators B*, **1999**, 61(1–3), 170–182.
58 T. Nakamoto, A. Iguchi, T. Moriizumi. *Sens. Actuators B*, **2000**, 71, 155–160.
59 E. Llobet, X. Villanova, J. Brezmes, R. Alcubilla, J. Calderer, J. E. Sueiras, J. Correig. *Meas. Sci. Technol.*, **1997**, 8, 1133–1138.
60 G. E. P. Box, D. R. Cox. *J. Roy. Statist. Soc. Ser. B*, **1964**, 26, 211–243.
61 F. Bordoni, A. D'Amico. *Sens. Actuators A*, **1990**, 21–23, 17–24.
62 P. Corcoran. *Sens. Actuators B*, **1994**, 18–19, 649–653.
63 H. Ulmer, J. Mitrovics, U. Weimar, W. Göpel. *Sens. Actuators B*, **2000**, 65(1–3), 79–81.
64 J. W. Grate, S. L. Rose-Pehrsson, D. L. Venezky, M. Klusty, H. Wohltjen. *Anal. Chem.*, **1993**, 65, 1868–1881.
65 B. Hivert, M. Hoummady, D. Hauden, P. Mielle, G. Mauvais, J. M. Henrioud. *Sens. Actuators B*, **1995**, 27(1–3), 242–245.
66 S. Strathmann. *Sample Conditioning for Multi-Sensor Systems*, Ph.D. Dissertation,

Institute for Physical and Theoretical Chemistry, University of Tübingen, Germany, **2001**.
67 U. Weimar, W. Göpel. *Sens. Actuators B*, **1998**, 52, 143–161.
68 M. J. Madou, S. R. Morrison. *Chemical Sensing with Solid State Devices*, Academic Press, Boston, MA, **1989**.
69 A. P. Lee, B. J. Reedy. *Sens. Actuators B*, **1999**, 60, 35–42.
70 N. Yamazoe, N. Miura. In *Chemical Sensor Technology Vol. 4* (Ed.: S. Yamauchi), Chemical Sensor Technology, **1992**, 19–42.
71 S. Nakata, S. Akakabe, M. Nakasuji, K. Yoshikawa. *Anal. Chem.*, **1996**, 68, 2067–2072.